Research Square

Preprints are preliminary reports that have not undergone peer review.
They should not be considered conclusive, used to inform clinical practice,
or referenced by the media as validated information.

Recycled $LiMn_2O_4$ Cathode–Graphite Composite as an Electrochemical Sensor for Hydrogen Peroxide

Eric M. Garcia

eric@ufsj.edu.br

Federal University of São João del-Rei

Hosane A. Taroco

Federal University of São João del-Rei

Julio O. F Melo

Federal University of São João del-Rei

Ana P.C.M. Silva

Federal University of São João del-Rei

Renata P. L. Moreira

Universidade Federal de Viçosa

Short Report

Keywords: Li-ion battery, recycling, glucose sensor, cooper

Posted Date: November 18th, 2026

DOI: https://doi.org/10.21203/rs.3.rs-11587471/v1

License: This work is licensed under a Creative Commons Attribution 4.0 International License.
Read Full License

Additional Declarations: No competing interests reported.

Recycled $LiMn_2O_4$ Cathode–Graphite Composite as an Electrochemical Sensor for Hydrogen Peroxide

Eric M. Garcia (Corresponded author)[1], Hosane A. Taroco[1], Julio O. F Melo[1], Ana P.C.M. Silva, Renata P. L. Moreira[2]

1) **DECEB** - Department of Exact and Biological Sciences - Federal University of São João del-Rei **(UFSJ) City :** Sete lagoas. **State** : Minas Gerais. **Country :** Brazil.

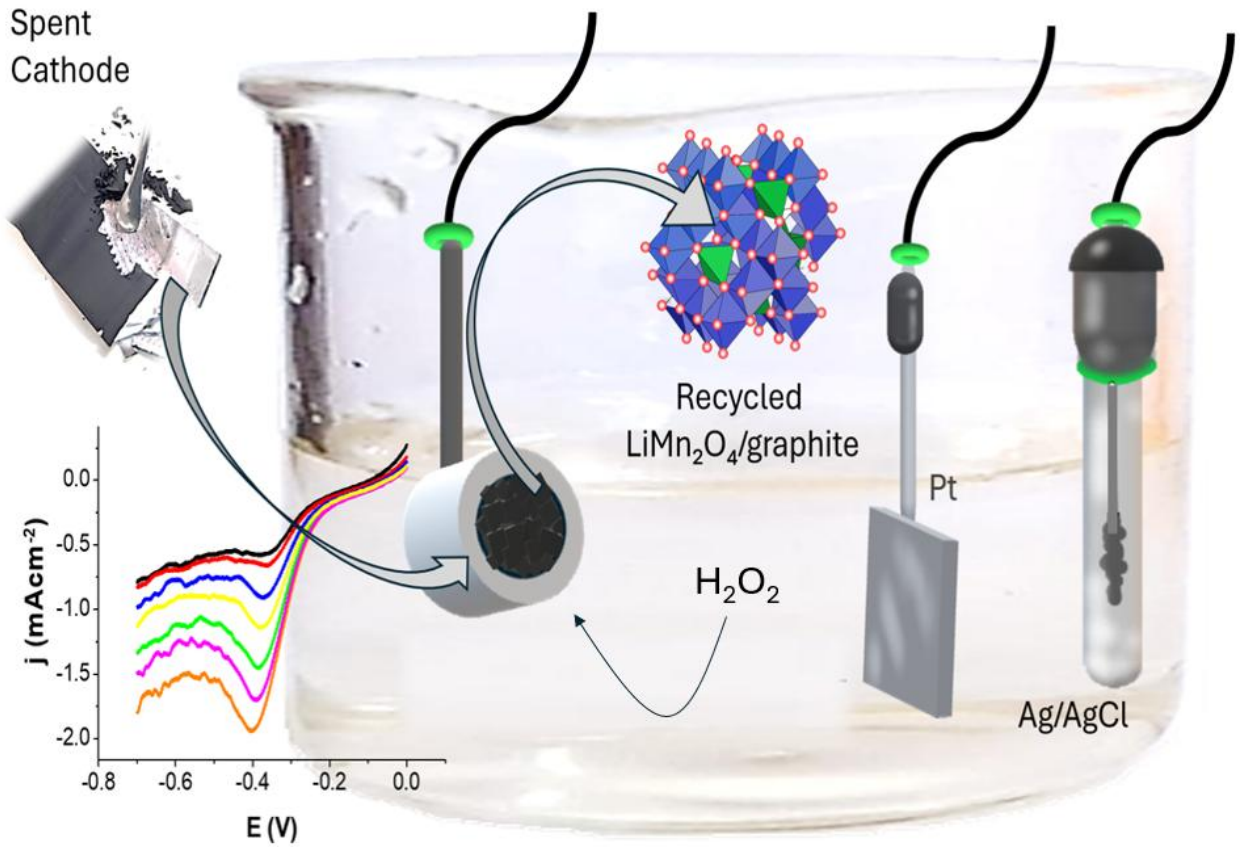
2) **DEQ –** Department of Chemical Engineering**,** Federal University of Viçosa **(UFV). City:** Viçosa. **State:** Minas Gerais. **Country:** Brazil.

E-mail: renata.plopes@ufv.br

Keywords: Li-ion battery, recycling, glucose sensor, cooper

Corresponded author e-mail : eric@ufsj.edu.br

Graphical Abstract



Abstract :

The direct reuse of spent lithium-ion battery cathodes as functional electrochemical materials offers a promising strategy for waste valorization. In this study, $LiMn_2O_4$ recovered from discarded mobile phone batteries was investigated for electrochemical hydrogen peroxide (H_2O_2) detection. The recovered material, characterized by a predominantly spinel structure, was incorporated into a simple graphite–mineral oil composite without noble-metal catalysts or advanced carbon nanomaterials. In 0.1 mol L^{-1} NaOH, the electrode exhibited a pronounced cathodic response near −0.39 V vs. Ag/AgCl upon H_2O_2 addition, whereas the graphite control showed no comparable enhancement. A highly linear response was obtained over 0–1.370 mmol L^{-1} (R = 0.99986), with a sensitivity of 980.65 μA mM^{-1} cm^{-2} and an estimated detection limit of 29.11 μmol L^{-1}. The enhanced response may involve peroxide reduction facilitated by manganese redox-active sites. These findings demonstrate the potential of recycled $LiMn_2O_4$ as an electroactive sensing material, providing a simple route for converting spent battery cathodes into value-added electrochemical devices.

Keywords: Li-ion battery, recycling, hydrigen peroxide sensor, $LiMn_2O_4$

Corresponded author e-mail : eric@ufsj.edu.br

1. Introduction

Lithium-ion batteries (LIBs) have represented a major revolution in energy storage since their commercialization in the early 1990s. Currently, their applications range from portable electronic devices to electric vehicles, driven by characteristics such as high energy density, good charge retention, a wide operating temperature range, and excellent cycling performance. With the rapid expansion of the electric vehicle market, the global fleet is expected to reach approximately 130 million vehicles by 2030, generating around 11 million tons of lithium-ion battery waste [1,2]. The cathodes of these batteries are mainly composed of lithium-containing transition-metal compounds, such as $LiCoO_2$ (LCO), $LiMn_2O_4$ (LMO), $LiNi_xMn_yCo_{1-x-y}O_2$ (NMC), $LiNi_xCo_yAl_{1-x-y}O_2$ (NCA), and $LiFePO_4$ (LFP), depending on the battery chemistry. Thus, recycling lithium-ion batteries can play a critical role in reducing the pressure associated with the extraction of critical metals such as Li, Co, Ni, and Mn [3].

Among the different strategies investigated for the recycling of spent lithium-ion batteries, hydrometallurgical routes based on selective precipitation or co-precipitation have been widely employed for the recovery of valuable metals from cathode leachates. In these processes, metals such as Co, Ni, Mn, and Li can be recovered as hydroxides, carbonates, phosphates, or other precursor compounds, which may subsequently be reused for the synthesis of new battery materials [4,5]. Electrochemical approaches have also attracted increasing attention because they enable the recovery of metals directly from solution, for example through electrodeposition of metallic Co or Cu and electrochemical oxidation of Mn species, potentially reducing the use of additional chemical

reagents [6,7]. More recently, direct recycling and upcycling strategies have emerged as promising alternatives, aiming to preserve or reuse the intrinsic chemical and structural value of spent cathode materials instead of completely converting them into individual metal salts. In this context, recovered cathode oxides can be regenerated, directly reused, or transformed into functional materials for applications beyond batteries [8–10].

In the literature, several studies have demonstrated the direct reuse of recycled $LiMn_2O_4$-based cathode materials in applications beyond battery regeneration [11–15]. More broadly, recent studies have highlighted the upcycling of spent Li-ion battery cathodes into functional materials for adsorption, catalytic oxidation, photocatalysis, and electrocatalytic environmental remediation, reinforcing the potential of recycled cathode oxides for diverse applications [11–15]. In addition, spent $LiMn_2O_4$ cathodes have been directly applied to the oxidative decolorization of indigo carmine without the addition of H_2O_2 or UV irradiation, taking advantage of the Mn^{3+}/Mn^{4+} redox chemistry of the spinel structure [13]. Furthermore, the catalytic activity of $LiMn_2O_4$ in H_2O_2-mediated oxidation processes has been reported in the literature [15], potentially involving the redox chemistry of manganese.

In this context, another promising application of recycled $LiMn_2O_4$ is the electrochemical detection of hydrogen peroxide (H_2O_2), since the Mn^{3+}/Mn^{4+} redox couple may facilitate electron-transfer processes associated with H_2O_2 reduction. In the present study, $LiMn_2O_4$ recovered from spent mobile phone batteries was investigated as an electroactive material for H_2O_2 detection. The electrode was prepared using a simple composite of recycled $LiMn_2O_4$, graphite, and light mineral oil, without the addition of polymeric binders such as Nafion or

advanced conductive materials such as carbon nanotubes or graphene. This approach provides a straightforward and potentially low-cost strategy for converting spent battery cathode materials into electrochemical sensing platforms.

2. Experimental

2.1 Recovery of $LiMn_2O_4$ from Spent Lithium-Ion Battery Cathode Powder (SLBCP)

Spent Li-ion battery cathode powder (SLBCP) was obtained from disassembled commercial Nokia BL-4C cellphone batteries. This battery model was selected based on its expected manganese-based cathode chemistry, which was subsequently confirmed by X-ray diffraction (XRD) to consist predominantly of $LiMn_2O_4$. The battery cells were manually dismantled, and their main components, including the steel casing, separator, anode, and cathode, were separated using bench tools.

To remove residual electrolyte and polymeric binder and facilitate the detachment of the active material from the aluminum current collector, the cathodes were thermally treated at 400 °C for 24 h in a muffle furnace [15,16]. After thermal treatment, the cathodic powder was manually separated from the aluminum foil and washed with deionized water under magnetic stirring for 30 min to remove soluble residual species. The resulting solid was subsequently air-dried for 24 h.

The crystalline phases of the recovered cathode material were characterized by X-ray diffraction (XRD) using a Rigaku Rotaflex 200B diffractometer equipped with Cu Kα radiation and a Co filter. The measurements were performed using a scan rate of 0.02° min^{-1}. XRD analysis confirmed $LiMn_2O_4$ as the predominant crystalline phase in the recovered material. The overall procedure used for cathode recovery is schematically illustrated in Figure 1.

The textural properties of the recovered cathode powder were evaluated by nitrogen adsorption–desorption measurements at 77.35 K using a NOVA 600 surface area and pore size analyzer (Anton Paar). The samples were placed in 9 mm analysis cells and subjected to vacuum degassing prior to analysis. The specific surface area was determined using the multipoint Brunauer–Emmett–Teller (BET) method based on the adsorption branch of the N_2 isotherms.

The morphology and elemental composition of the recovered cathode powder were investigated by scanning electron microscopy coupled with energy-dispersive X-ray spectroscopy (SEM/EDS). Analyses were performed using an FEI Quanta 450 FEG microscope operated at 20 kV at the Mechanical Engineering Department of the Federal University of São João del-Rei (UFSJ). SEM was used to examine particle morphology and surface characteristics, whereas EDS provided qualitative and semi-quantitative information on the elemental composition of the recovered cathode material.

Particle size distribution and zeta potential measurements were performed using a Malvern Zetasizer instrument at 25 °C. The recovered cathode powder was dispersed in deionized water and sonicated in an ultrasonic bath for 30 min

prior to analysis to promote particle dispersion and minimize agglomeration. Particle size distributions were determined by dynamic light scattering (DLS), whereas zeta potential measurements were conducted at different pH values to evaluate the pH-dependent electrokinetic surface properties of the recycled material.

2.1. Preparation of the $LiMn_2O_4$–graphite composite electrode (LGC)

The $LiMn_2O_4$–graphite composite (LGC) was prepared by mixing 0.5 g of recycled $LiMn_2O_4$, 0.5 g of graphite powder, and 1.0 g of light mineral oil (Sigma-Aldrich, M8410). The mixture was homogenized under magnetic stirring for 1 h and subsequently applied to the surface of a graphite electrode using a brush. For comparison purposes, a graphite composite (GC) electrode was prepared following the same procedure, but without the addition of $LiMn_2O_4$.

Electrochemical measurements were performed in a conventional three-electrode cell containing 0.1 mol L^{-1} NaOH as the supporting electrolyte. The LGC-modified graphite electrode was used as the working electrode, a platinum electrode as the counter electrode, and a saturated Ag/AgCl electrode as the reference electrode. Linear sweep voltammetry (LSV) was performed in the absence and presence of H_2O_2, while chronoamperometric measurements were carried out at −0.50 V vs. Ag/AgCl, with successive additions of H_2O_2.

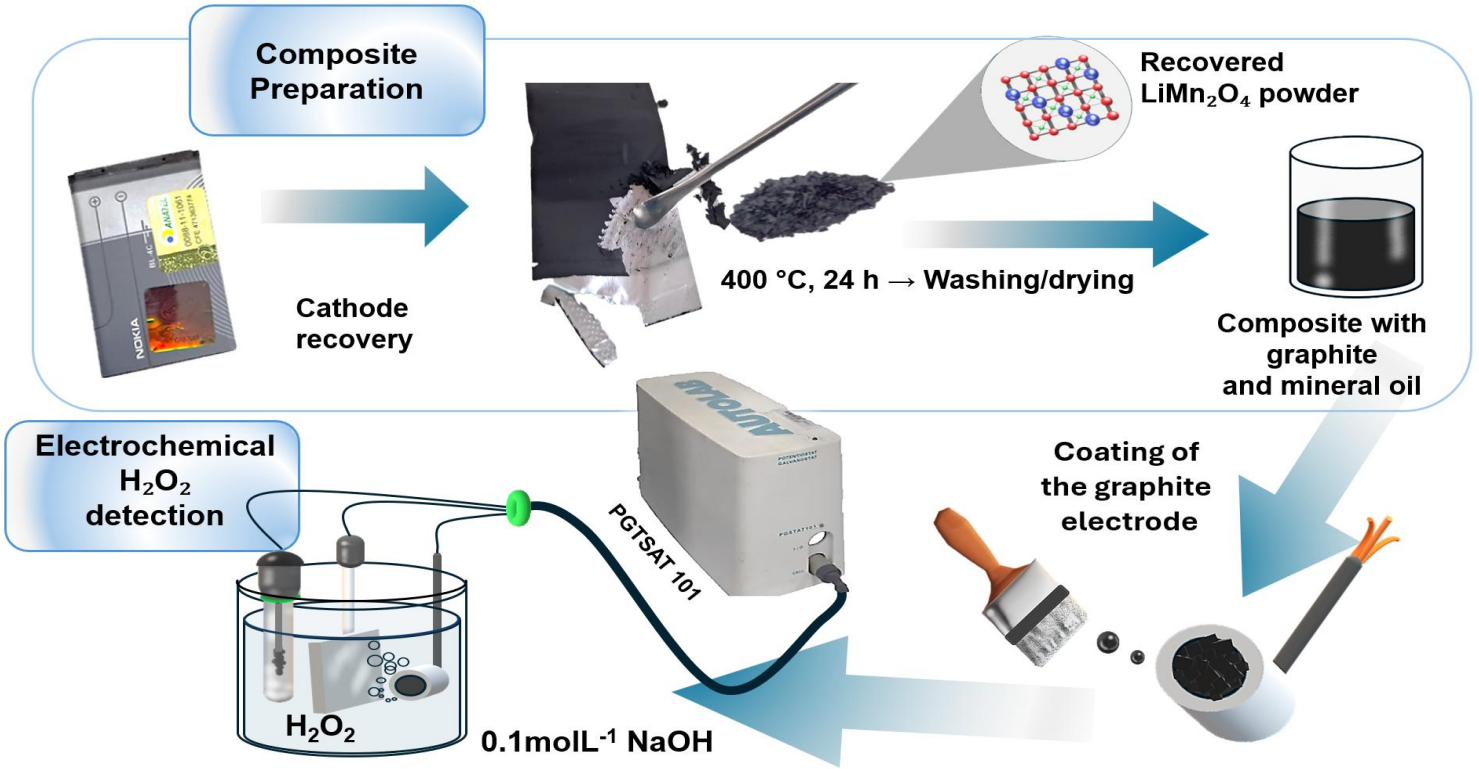


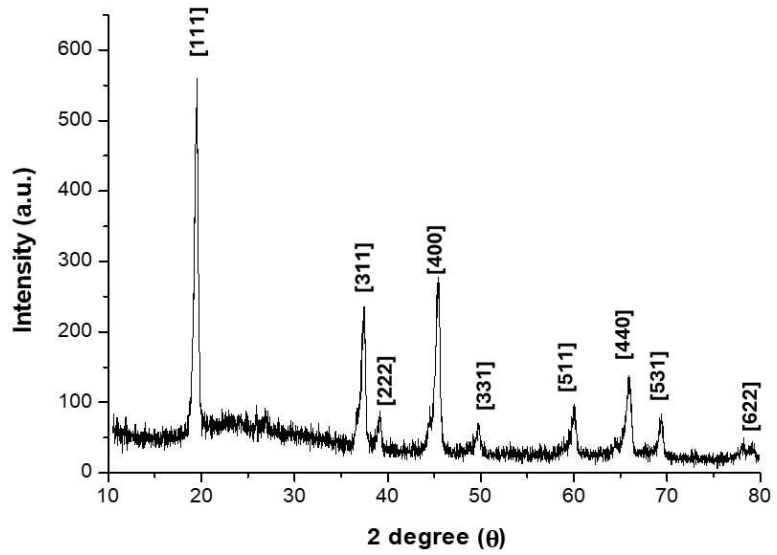
Figure 1- Schematic overview of the preparation and use of SLBCP (Spent Li-ion Battery Cathode Powder) as a catalyst. Li-ion batteries were manually dismantled, and the cathode material was thermally treated, mechanically removed, washed, and

3. Results

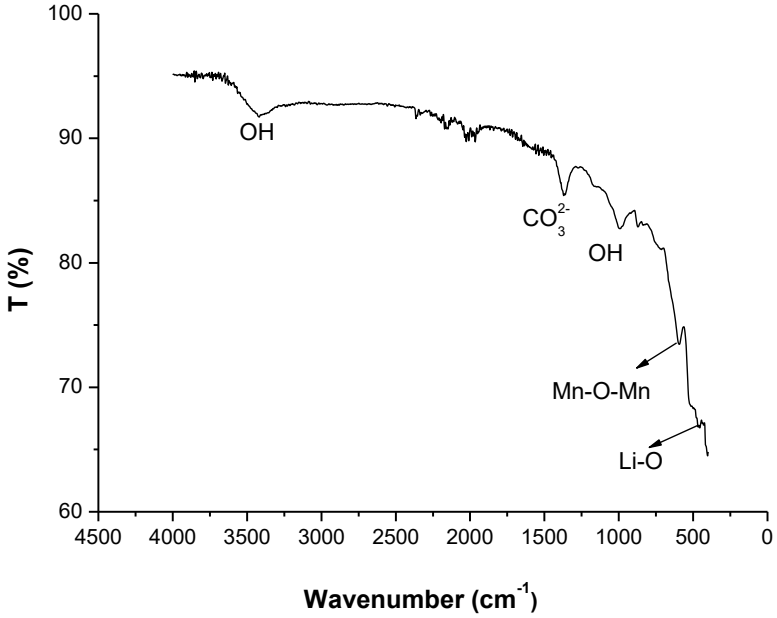
3.1 Characterization of SLBCP

Figure 2 -a shows the powder X-ray diffraction (XRD) pattern of the recycled spent Li-ion battery cathode powder (SLBCP) before its reaction with Sunset Yellow (SY) under acidic conditions (pH 1.5). The main diffraction peaks observed at approximately 19°, 36°, 38°, 44°, 48°, 58°, 64°, 67°, and 76° can be indexed to the (111), (311), (222), (400), (331), (511), (440), (531), and (622) planes, respectively, confirming the presence of the cubic spinel $LiMn_2O_4$ phase. This assignment is consistent with the cubic spinel structure reported for $LiMn_2O_4$ in the literature [16-18].

The FTIR spectrum of the recycled cathode material exhibited absorption bands in the low-wavenumber region characteristic of spinel $LiMn_2O_4$ (Figure 2-b). Previous studies have reported characteristic bands at approximately 615 and 510 cm^{-1}, assigned to Mn–O vibrations within the MnO_6 octahedral units of the $LiMn_2O_4$ spinel structure [18-27]. Similar low-wavenumber features have also been reported for spent cathode materials containing $LiMn_2O_4$ [26]. An additional absorption feature around 1000–1100 cm^{-1} may be associated with surface hydroxyl species and/or adsorbed water. Similar OH-related bands have been reported for spent LCO/LMO cathode materials [26]. A further band observed at approximately 1370 cm^{-1} may be attributed to surface carbonate species [27], which may arise from interaction of the cathode surface with atmospheric CO_2 and moisture during handling or storage [28].



(a)



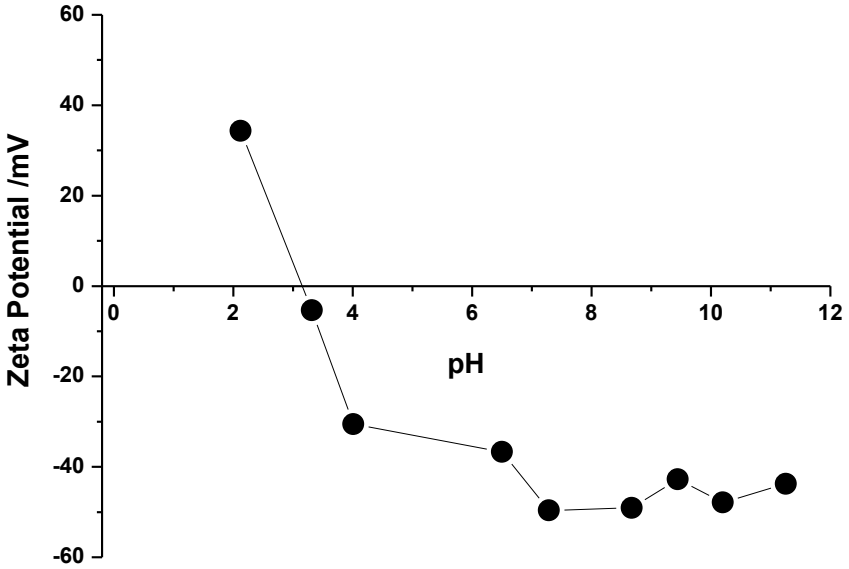
(b)

Figure 2. (a) XRD pattern of the recycled cathode material, showing the characteristic reflections of spinel $LiMn_2O_4$; (b) FTIR spectrum showing the main vibrational bands of the material.

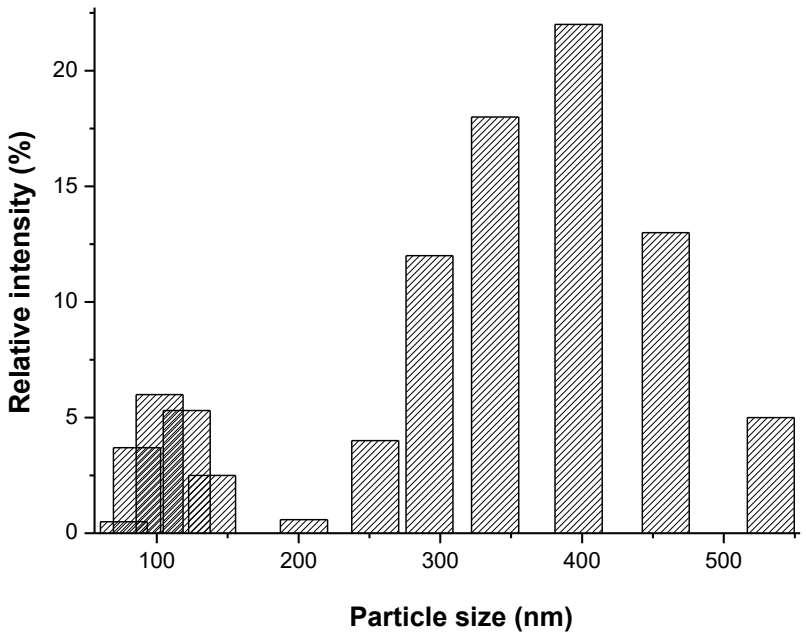
Figure 3-a shows the zeta potential of the recycled cathode material obtained from spent Li-ion batteries as a function of pH. The surface charge strongly depends on the solution pH, changing from positive values under highly acidic conditions to negative values as the pH increases. At pH ≈ 1.5, the zeta potential is approximately +35 mV, while the isoelectric point (IEP), where the zeta potential approaches zero, is observed at approximately pH 2.7–3.0. Above this pH, the surface becomes negatively charged, with the zeta potential decreasing to approximately −45 to −50 mV at neutral and alkaline pH values. This pH-dependent behavior is consistent with the protonation and deprotonation of surface hydroxyl groups commonly observed in metal oxides [11,29,30].

Figure 3-b shows the particle size distribution of the recycled cathode material. The sample exhibits a relatively broad particle size distribution, with the main population located between approximately 300 and 450 nm and a maximum relative intensity around 400 nm. A smaller population of particles is also observed in the 80–150 nm range, indicating a polydisperse particle size distribution.

Figure 4 shows the SEM micrograph and EDS spectrum of the recycled cathode material. The SEM image reveals particles with irregular morphology and a heterogeneous size distribution, together with interparticle voids that give the material a relatively rough and loosely packed appearance. The EDS spectrum indicates Mn and O as the predominant elements, consistent with the $LiMn_2O_4$ phase identified by XRD. Carbon may be associated with residual conductive carbon from the original cathode composite, while the presence of F is likely related to fluorinated residues from the battery components, particularly $LiPF_6$-derived electrolyte species and/or PVDF binder residues.

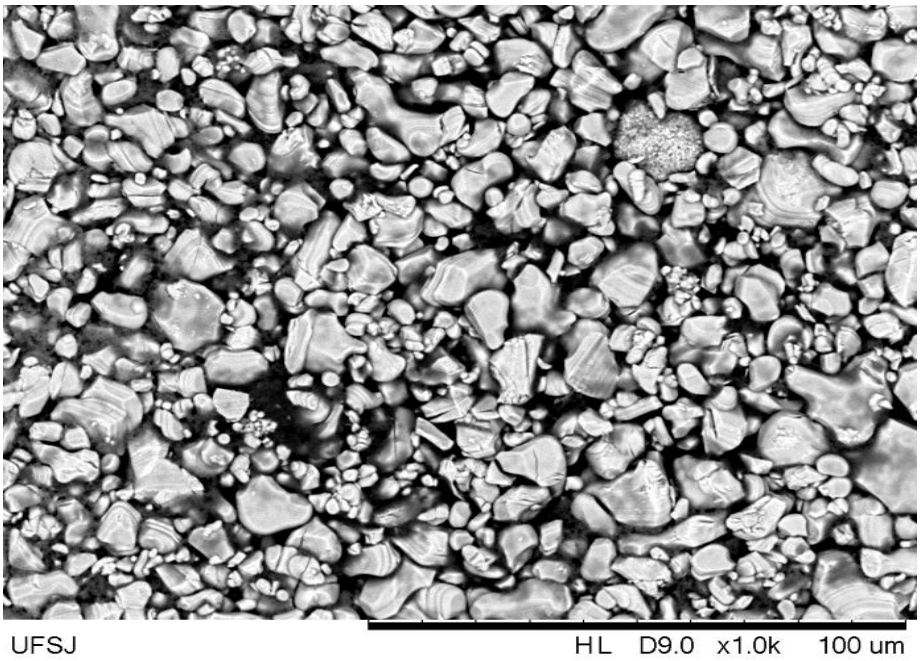


(a)

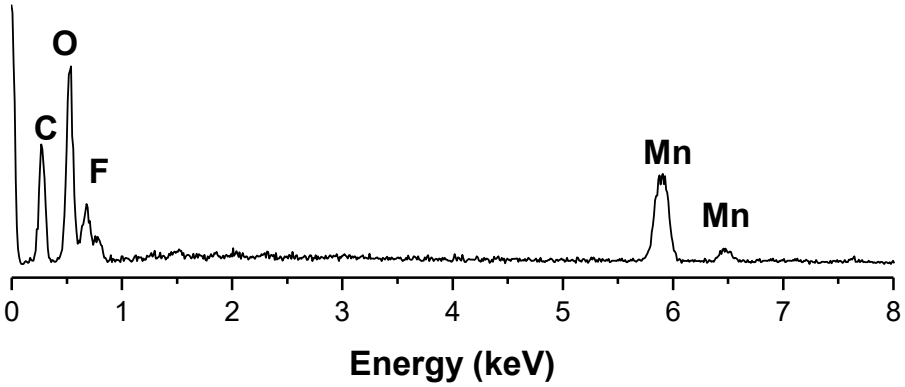


(b)

Figure 3. (a) Zeta potential as a function of pH and (b) particle size distribution of the recycled spent Li-ion battery cathode material.



(a)



(b)

Figure 4. (a) SEM micrograph showing the morphology of the recycled cathode material and (b) corresponding EDS spectrum, indicating the presence of Mn, O, C, and F.

Figure 5 shows the N_2 adsorption–desorption isotherm of the recycled cathode material. The sample exhibited a relatively low BET specific surface area of 1.624 $m^2\ g^{-1}$. A hysteresis between the adsorption and desorption branches is observed, particularly at higher relative pressures, together with a pronounced increase in N_2 uptake as P/P_0 approaches 1. The BJH analysis indicated a pore volume of 0.00287 $cm^3\ g^{-1}$ and a characteristic pore diameter of approximately 3.84 nm, suggesting the presence of mesopores (Table 1).

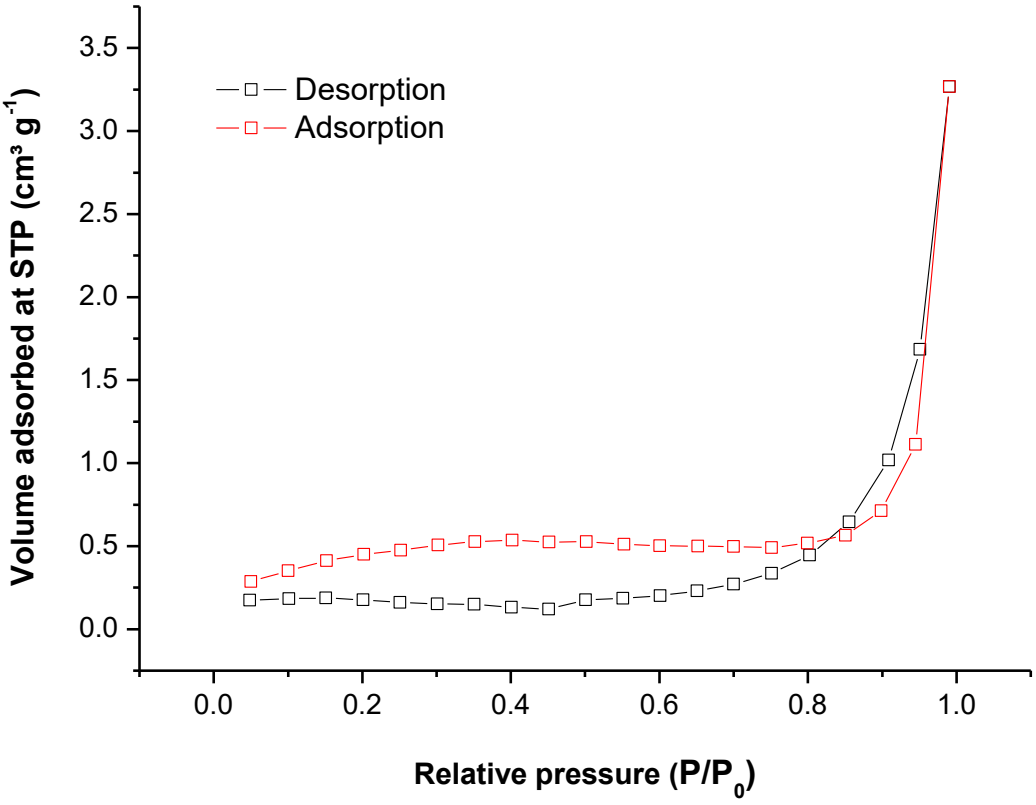


Figure 5. N_2 adsorption–desorption isotherm of the recycled cathode material, showing the hysteresis between adsorption and desorption branches at 77 K.

Table 1. Textural properties of the cathode material determined by N_2 adsorption–desorption measurements.

Sample	BET surface area ($m^2\ g^{-1}$)	BJH pore volume ($cm^3\ g^{-1}$)	BJH pore diameter (nm)
Recycled cathode	1.624	0.00287	3.84

Figure 6 shows the linear sweep voltammograms obtained using the $LiMn_2O_4$–graphite composite (LGC) and graphite (GC) electrodes in 0.1 mol L^{-1} NaOH, in the absence and presence of 0.4 mmol L^{-1} H_2O_2. In the absence of H_2O_2, the LGC electrode exhibited a distinct cathodic response compared with the GC electrode, suggesting that the incorporation of recycled $LiMn_2O_4$ promotes additional electrochemical processes, possibly associated with dissolved oxygen reduction (Eq. 1).

$$O_2 + H_2O + 2e^- \rightarrow HO_2^- + OH^- \quad (Eq.1)$$

Upon H_2O_2 addition, a pronounced cathodic peak appeared at approximately −0.39 V, whereas the graphite electrode showed no comparable enhancement. This result indicates that the incorporation of recycled $LiMn_2O_4$ significantly promotes the peroxide-dependent cathodic response. In alkaline medium, oxygen reduction and hydroperoxide reduction may occur concomitantly, according to the reaction (Eq.2):

$$HO_2^- + H_2O + 2e^- \rightarrow 3OH^- \quad (Eq.\,2)$$

The enhanced cathodic response may therefore arise from peroxide-related reduction processes facilitated by manganese-containing surface sites. Similar simultaneous oxygen and peroxide reduction pathways have been discussed for manganese-based oxide electrodes [31].

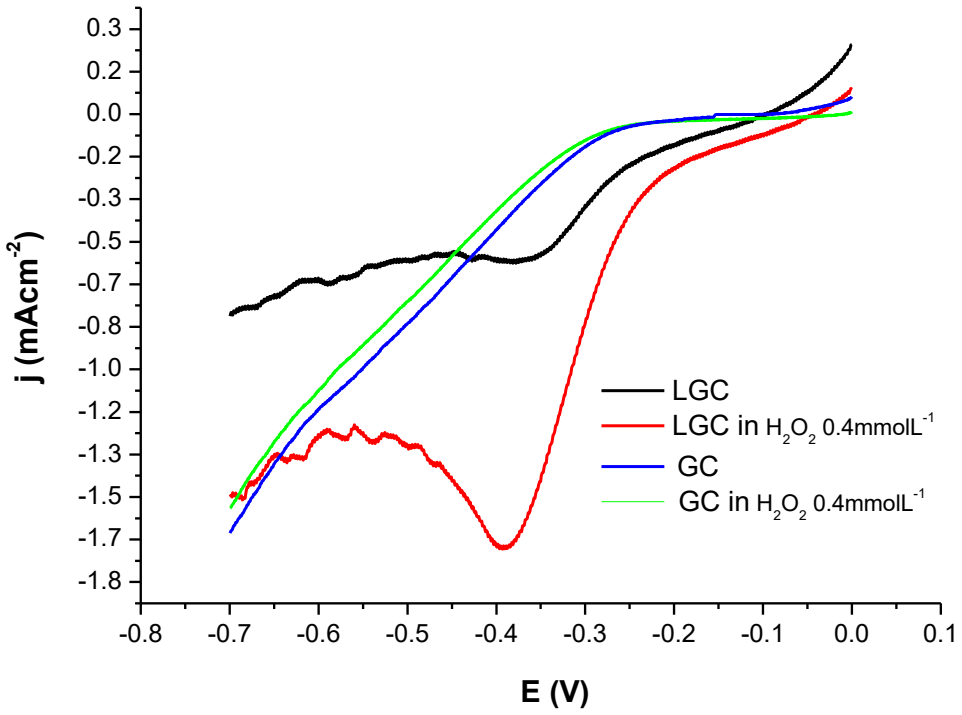
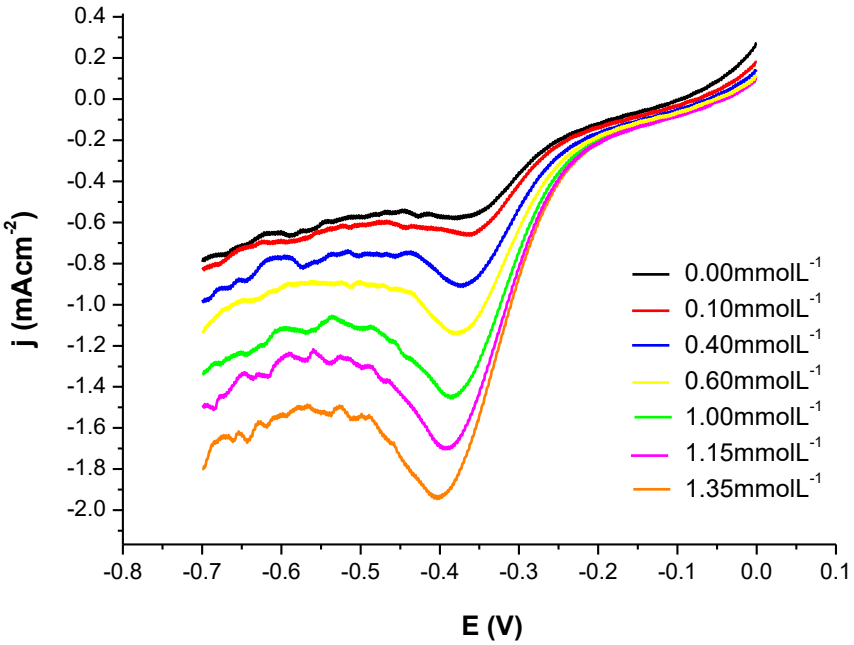


Figure 6. Linear sweep voltammograms obtained using the $LiMn_2O_4$–graphite composite (LGC) and graphite composite (GC) electrodes in 0.1 mol L^{-1} NaOH, in the absence and presence of 0.4 mmol L^{-1} H_2O_2.

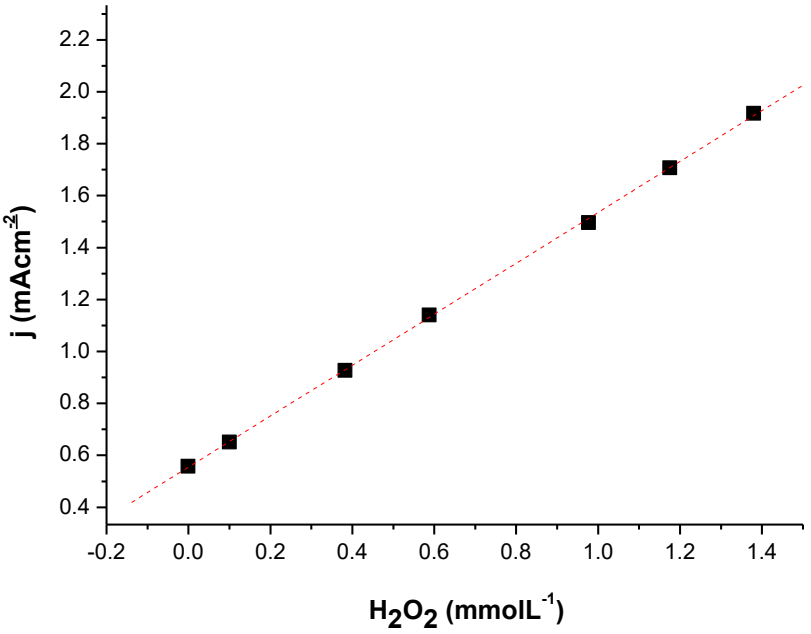
The electrocatalytic activity of $LiMn_2O_4$ may also be associated with the Mn^{4+}/Mn^{3+} redox couple present in its spinel structure. Under cathodic polarization, Mn^{4+} surface centers may undergo electrochemical reduction to Mn^{3+}, potentially facilitating electron transfer to peroxide species (Eq.3). The subsequent reoxidation of Mn^{3+} to Mn^{4+} could regenerate the active sites, establishing a possible redox-mediated catalytic cycle. Such a mechanism may provide a kinetically favorable pathway for peroxide reduction, contributing to the enhanced cathodic response observed at the LGC electrode.

$$2\mathrm{Mn}^{\mathrm{III}}_{\mathrm{surf}} + \mathrm{HO}_2^- + \mathrm{H_2O} \rightarrow 2\mathrm{Mn}^{\mathrm{IV}}_{\mathrm{surf}} + 3\mathrm{OH}^- \quad (Eq.3)$$

Figure 7(a) shows the linear sweep voltammograms recorded at the LGC electrode upon successive increases in H_2O_2 concentration from 0 to 0.400 mmol L^{-1}. A progressive increase in the cathodic peak current density was observed, with the peak located at approximately −0.40 V vs. Ag/AgCl. The magnitude of the cathodic current increased systematically with H_2O_2 concentration, indicating a concentration-dependent electrochemical response. As shown in Figure 7(b), the cathodic peak current density exhibited an approximately linear relationship with H_2O_2 concentration over the investigated range, supporting the applicability of the recycled $LiMn_2O_4$–graphite composite for electrochemical H_2O_2 detection.



(a)



(b)

Figure 7. (a) Linear sweep voltammograms recorded at the $LiMn_2O_4$–graphite composite (LGC) electrode in 0.1 mol L^{-1} NaOH with increasing H_2O_2 concentrations (0–0.400 mmol L^{-1}); (b) corresponding calibration curve of cathodic peak current density as a function of H_2O_2 concentration.

Table 2 compares the analytical performance of the recycled $LiMn_2O_4$–graphite composite (LGC) with previously reported manganese oxide-based electrodes for electrochemical H_2O_2 detection. The LGC electrode exhibited a sensitivity of 980.65 μA mM^{-1} cm^{-2} over the concentration range of 0–1.370 mM, with an estimated detection limit of 29.11 μM. Although some previously reported sensors exhibited higher sensitivities and lower detection limits, the LGC electrode demonstrated a highly linear response to H_2O_2 concentration (R = 0.99986), with a sensitivity comparable to or higher than those reported for several manganese oxide-based electrodes, including Bi_2O_3/MnO_2 (914.0 μA mM^{-1} cm^{-2}) and MnO–Mn_3O_4/rGO (274.15 μA mM^{-1} cm^{-2}). Importantly, this analytical response was achieved using recycled $LiMn_2O_4$ incorporated into a simple graphite–mineral oil composite, without noble-metal nanoparticles, graphene, or carbon nanotubes. These findings highlight the potential of recycled battery cathode materials as electroactive components for H_2O_2 detection. Nevertheless, differences in electrochemical techniques, electrode configurations, and experimental conditions should be considered when comparing the reported analytical performances.

Table 2. Comparison of the analytical performance of manganese oxide-based electrodes for electrochemical H_2O_2 detection.

Electrode material	Linear range (mM)	LOD (μM)	Sensitivity (μA mM^{-1} cm^{-2})	Reference
MnO_2/MWCNTs	0.100–20.5	6.97	13.9	[32]
δ-MnO_2/CNTs	0.050–22.0	1.00	243.9	[33]
MnO–Mn_3O_4/rGO	0.004–17.0	0.10	274.15	[34]
Ag/δ-MnO_2/graphene	0.005–90.64	0.068	104.43	[35]
MnO–CrN	0.00033–15.0	0.059	2156.25	[36]
Bi_2O_3/MnO_2	0.0002–0.290	0.050	914.0	[37]
Recycled $LiMn_2O_4$/graphite (LGC)	0–1.370	29.11	980.65	This work

Although the estimated detection limit of the LGC electrode is higher than those reported for several manganese oxide-based sensors, its relatively high sensitivity (980.65 μA mM^{-1} cm^{-2}) highlights the potential of recycled $LiMn_2O_4$ as an electroactive material for H_2O_2 detection. Sensitivity reflects the change in electrochemical response with analyte concentration and is influenced by the electrocatalytic properties of the electrode material, as well as its surface

characteristics and mass transport conditions. The pronounced enhancement in cathodic current observed upon incorporating $LiMn_2O_4$, compared with the graphite control electrode, suggests that manganese-containing sites contribute to the peroxide-dependent response. Therefore, despite the comparatively higher detection limit, the results demonstrate the potential of recycled $LiMn_2O_4$ for developing electrochemical sensing platforms with competitive analytical sensitivity.

4. Conclusion

This study demonstrated the potential of $LiMn_2O_4$ recovered from spent lithium-ion batteries as an electroactive material for hydrogen peroxide detection. The recovered cathode powder retained the characteristic spinel structure of $LiMn_2O_4$ and was successfully incorporated into a simple graphite–mineral oil composite electrode. Compared with the graphite control, the $LiMn_2O_4$-containing electrode showed a pronounced enhancement in cathodic current upon H_2O_2 addition, indicating that the recycled manganese oxide actively contributes to the peroxide reduction process. The electrode exhibited a highly linear response over the concentration range of 0–1.370 mmol L^{-1} ($R = 0.99986$), with a sensitivity of 980.65 μA mM^{-1} cm^{-2} and an estimated detection limit of 29.11 μmol L^{-1}. Although the detection limit is higher than those reported for some advanced H_2O_2 sensors, the competitive sensitivity achieved with a simple composite containing recycled $LiMn_2O_4$ highlights the potential of this material for electrochemical sensing. The observed cathodic behavior may involve contributions from both oxygen and

peroxide reduction, potentially assisted by the Mn^{3+}/Mn^{4+} redox chemistry of the spinel structure. Overall, these results demonstrate the feasibility of directly reusing recovered $LiMn_2O_4$ in electrochemical sensing platforms, providing a simple, potentially low-cost, and value-added route for the valorization of spent lithium-ion battery cathodes.

Data availability statement : The authors declare that the data supporting the findings of this study are available within the paper.

Interest Statement : The authors declare that they have no conflict of interest

Funding Declaration : The authors declare that they were not funded by any organization or fund.

Author Contribution: E.M.G., H.A.T., J.O.F.M., and A.P.C.M. performed the electrochemical experiments and contributed to data analysis and interpretation. R.P.L.M. contributed to the BET surface area and porosity characterization. All authors contributed to the manuscript preparation, discussed the results, reviewed the manuscript, and approved the final version for submission.

Consent to Publish declaration: Not applicable.

Consent to Participate declaration: Not applicable.

Ethics declaration: Not applicable.

5 Reference

[1] Apte, S.; Mukherjee, A.; Mishra, P. Sustainable metal recovery from spent lithium-ion battery using electrochemical technique: A comprehensive method review. *MethodsX*, **15**, 103506, 2025. https://doi.org/10.1016/j.mex.2025.103506

[2] Paul, S.; Shrotriya, P. Efficient Recycling Processes for Lithium-Ion Batteries. *Materials*, **18**, 613, 2025. https://doi.org/10.3390/ma18030613

[3] Lach, M.; Przybek, A.; Duda, P.; Bielaczyc, P. A Review of Direct Recycling Processes for Lithium-Ion Battery Cells. *Materials*, **18**, 5608, 2025. https://doi.org/10.3390/ma18245608

[4] Tawonezvi, T.; Nomnqa, M.; Petrik, L.; Bladergroen, B. J. Recovery and Recycling of Valuable Metals from Spent Lithium-Ion Batteries: A Comprehensive Review and Analysis. *Energies*, **16**, 1365, 2023. https://doi.org/10.3390/en16031365

[5] Gu, S.; Kong, J.; Fang, B. Comprehensive recycling of spent lithium-ion battery cathodes and anodes via a targeted electrochemical redox process. *Green Chemistry*, **26**, 4484, 2024. https://doi.org/10.1039/D4GC00163J

[6] Wang, Z.; Chen, Y.; Zhou, F.; Qin, R.; Tian, Y.; Xue, Z.; Mu, T. Upcycling spent lithium-ion battery cathodes into cobalt-polyphenol networks by DES dissolution and solvent-induced crystallization. *Green Chemistry*, **26**, 5988, 2024. https://doi.org/10.1039/D4GC01036A

[7] Xu, B.; Díez, N.; Sevilla, M.; Ferrer, M. L.; Gutiérrez, M. C.; del Monte, F. Recycling and Reutilization of Metals Aided by Deep Eutectic Solvents: From NMC Cathodes of Spent Li-ion Batteries to Electrolytes for Supercapacitors. *ChemSusChem*, 2024. https://doi.org/10.1002/cssc.202401128

[8] Pražanová, A.; Plachý, Z.; Kočí, J.; Fridrich, M.; Knap, V. Direct Recycling Technology for Spent Lithium-Ion Batteries: Limitations of Current Implementation. *Batteries*, **10**, 81, 2024. https://doi.org/10.3390/batteries10030081

[9] Shrestha, A. B.; Amarasekara, A. S. The Sustainable and Green Management of Spent Lithium-Ion Batteries Through Hydroxy Acid Recycling and Direct Regeneration of Active Positive Electrode Material: A Review. *Batteries*, **11**, 68, 2025. https://doi.org/10.3390/batteries11020068

[10] Wang, Z.; Chen, Y.; Zhou, F.; Qin, R.; Tian, Y.; Xue, Z.; Mu, T. Upcycling spent lithium-ion battery cathodes into cobalt-polyphenol networks by DES dissolution and solvent-induced crystallization. *Green Chemistry*, **26**, 5988, 2024. https://doi.org/10.1039/D4GC01036A

[11] Garcia, E. M.; Dias, T. M.; Taroco, H. A.; Melo, J. O. F.; Mariz, C. S.; Rocha, F. A. Adsorptive removal of indigo carmine using recycled $LiMn_2O_4$ cathode material under non-redox conditions. *Discover Industrial Chemistry and Materials*, **1**, 11, 2026. https://doi.org/10.1007/s44508-026-00012-2

[12] Lima, L. T.; Garcia, E. M.; Taroco, H. A.; Melo, J. O. F.; Taroco, C. G. From waste to value: recycled Li-ion battery cathode catalyzes the transformation of sunset yellow into functional aromatics. *Ionics*, **32**, 289–306, 2026. https://doi.org/10.1007/s11581-025-06821-0

[13] Garcia, E. M.; Martins, T. D.; Taroco, H. A.; Melo, J. O. F.; Taroco, C. G. Oxidative decolorization of indigo carmine dye using spent cathode of Li-ion batteries. *Ionics*, **30**, 4647–4654, 2024. https://doi.org/10.1007/s11581-024-05612-3

[14] Feng, L.; Pan, C.; Zhang, B.; Liu, L.; Wan, J.; Cui, S.; Li, W. Fundamental research on recycling spent lithium-ion batteries for environmental pollutant control. *Journal of Environmental Management*, **394**, 127620, 2025. https://doi.org/10.1016/j.jenvman.2025.127620

[15] Long, Y.; Guo, J.; Huang, D.; Liu, G. Catalytic degradation of azo dye Congo red in aqueous solution by $LiMn_2O_4$. *Advanced Materials Research*, **634–638**, 500–503, 2013. https://doi.org/10.4028/www.scientific.net/AMR.634-638.500

[16] Xiang, J.; Zhang, P.; Lv, S.; Ma, Y.; Zhao, Q.; Sui, Y.; Ye, Y.; Qin, C. Spinel $LiMn_2O_4$ nanoparticles fabricated by the flexible soft template/Pichini method as cathode materials for aqueous lithium-ion capacitors with high energy and power density. *RSC Advances*, **11**, 14891, 2021. https://doi.org/10.1039/D0RA07823A

[17] Abdollahifar, M.; Huang, S.-S.; Lin, Y.-H.; Sheu, H.-S.; Lee, J.-F.; Lu, M.-L.; Liao, Y.-F.; Wu, N.-L. Tetragonal $LiMn_2O_4$ as dual-functional pseudocapacitor-battery electrode in aqueous Li-ion electrolytes. *Journal of Power Sources*, **412**, 545–551, 2019. https://doi.org/10.1016/j.jpowsour.2018.11.074

[18] Si, P.; Zheng, X.; Li, S.; Yang, Y.; Chen, L. Electrochemical characterization of nanostructured $LiMn_2O_4$ composite in Li-ion hybrid supercapacitors. *ChemElectroChem*, 2020. https://doi.org/10.1002/celc.202001198

[19] Huang, M.; Li, F.; Dong, F.; Zhang, Y. X.; Zhang, L. L. MnO_2-based nanostructures for high-performance supercapacitors. *Journal of Materials Chemistry A*, **3**, 21380, 2015. https://doi.org/10.1039/C5TA05523G

[20] Alves, A. C.; Correia, J. P.; Silva, T. M.; Montemor, M. F.; Taryba, M. In situ localized studies to unveil the charge storage mechanism of manganese oxide in

aqueous media. *Electrochimica Acta*, **519**, 145840, 2025. https://doi.org/10.1016/j.electacta.2025.1458

[21] Liu, J.; Bao, J.; Zhang, X.; Gao, Y.; Zhang, Y.; Liu, L.; Cao, Z. MnO_2-based materials for supercapacitor electrodes: challenges, strategies and prospects. *RSC Advances*, **12**, 35556, 2022. https://doi.org/10.1039/D2RA06664E

[22] Han, D.; Jang, H.; Choi, J.; Park, J.; Kim, S.; Han, S.; Lee, W.; Lee, J. H.; Oh, P.; Han, Y.; Park, M. Direct Integration of Spent $LiMn_2O_4$ with High Voltage Aqueous Zinc-Manganese Redox Flow Batteries as a Practical Upcycling Process. *Small*, 2025, 2500787. https://doi.org/10.1002/smll.202500787

[23] Liu, X.; Chen, Z.; Zhou, D.; Zhao, Q.; Feng, H.; Cui, Y.; Ding, C.; Gao, Y. Breaking the Specific Capacity Limit: 409% Boost in Manganese-Based Redox Flow Batteries at High Current Densities with a MnO_2 Semi-Solid Slurry Electrolyte. Nano-Micro Letters, 19, 41, 2027. https://doi.org/10.1007/s40820-026-02349-8

[24] Siqueira, J. M., Jr.; Machado, C. T.; Quattrociocchi, D. S. G.; Garrido, F. M. S.; da Costa, L. M.; Ponzio, E. A.; Ferreira, G. B.; Resende, J. A. L. C. Experimental and Theoretical Study of $LiMn_2O_4$ Synthesized by the Solution Combustion Method Using Corn Starch as Fuel. *Journal of the Brazilian Chemical Society*, **31**, 381–393, 2020. https://doi.org/10.21577/0103-5053.20190192

[25] Tariq, H. A.; Abraham, J. J.; Shakoor, R. A.; Al-Qaradawi, S.; Karim, M. R. A.; Chaudhry, U. Synthesis of lithium manganese oxide nanocomposites using microwave-assisted chemical precipitation technique and their performance evaluation in lithium-ion batteries. *Energy Storage*, 2020. https://doi.org/10.1002/est2.202

[26] Du, M.; Du, K.-D.; Guo, J.-Z.; Liu, Y.; Aravindan, V.; Yang, J.-L.; Zhang, K.-Y.; Gu, Z.-Y.; Wang, X.-T.; Wu, X.-L. Direct reuse of oxide scrap from retired lithium-ion batteries: advanced cathode materials for sodium-ion batteries. *Rare Metals*, **42**, 1603–1613, 2023. https://doi.org/10.1007/s12598-022-02230-8

[27] Charbonneau, V.; Larouche, F.; Amouzegar, K.; Soucy, G.; Veilleux, J. Quantification of hydroxide in co-precipitated nickel, manganese, cobalt carbonate precursor via TG-MS analyses. *Thermochimica Acta*, 2025. https://doi.org/10.1016/j.tca.2025.180035

[28] Sicklinger, J.; Metzger, M.; Beyer, H.; Pritzl, D.; Gasteiger, H. A. Ambient Storage Derived Surface Contamination of NCM811 and NCM111: Performance Implications and Mitigation Strategies. *Journal of The Electrochemical Society*, **166**(12), A2322–A2335, 2019. https://doi.org/10.1149/2.0011912jes

[29] Şahan, H.; Göktepe, H.; Patat, Ş.; Ülgen, A. Effect of the Cr_2O_3 coating on electrochemical properties of spinel $LiMn_2O_4$ as a cathode material for lithium battery applications. *Solid State Ionics*, **181**(31–32), 1437–1444, 2010. https://doi.org/10.1016/j.ssi.2010.08.008

[30] Nakayama, N.; Yamada, I.; Huang, Y.; Nozawa, T.; Iriyama, Y.; Abe, T.; Ogumi, Z. Effects of specific adsorption of copper(II) ion on charge transfer reaction at the thin film $LiMn_2O_4$ electrode/aqueous electrolyte interface. *Electrochimica Acta*, **54**(12), 3428–3432, 2009. https://doi.org/10.1016/j.electacta.2008.12.061

[31] Xavier, L. G. O.; Ebambi, T. C.; Diniz, R.; Lins, V. F. C.; Montoro, L. A.; Matencio, T. Enhanced Catalytic Performance of Strontium-Doped Lanthanum Manganites by the Presence of Molybdenum Oxides for Electro-Reduction of Hydrogen Peroxide. *Journal of the Brazilian Chemical Society*, **33**(6), 589–599, 2022. https://doi.org/10.21577/0103-5053.20220016

[32] Dinesh, M.; Revathi, C.; Haldorai, Y.; Kumar, R. T. R. Birnessite MnO_2 decorated MWCNTs composite as a nonenzymatic hydrogen peroxide sensor. *Chemical Physics Letters*, **731**, 136612, 2019. https://doi.org/10.1016/j.cplett.2019.136612

[33] Begum, H.; Ahmed, M. S.; Jeon, S. A novel δ-MnO_2 with carbon nanotubes nanocomposites as enzyme-free sensor for hydrogen peroxide electrosensing. *RSC Advances*, 2016. https://doi.org/10.1039/C6RA08738H

[34] Liu, Y.; Tang, L.; Deng, D.; He, H.; Yan, X.; Wang, J.; Luo, L. Hetero-structured MnO–Mn_3O_4@rGO composites: Synthesis and nonenzymatic detection of H_2O_2. *Materials Science and Engineering C*, 2020.

https://doi.org/10.1016/j.msec.2020.111443

[35] Mohiuddin, A. K.; Jeon, S. Highly efficient Ag doped δ-MnO_2 decorated graphene: Comparison and application in electrochemical detection of H_2O_2. *Applied Surface Science*, **592**, 153162, 2022. https://doi.org/10.1016/j.apsusc.2022.153162

[36] Tareen, A. K.; Khan, K.; Ahmad, W.; Khan, M. F.; Khan, Q. U.; Liu, X. A novel MnO–CrN nanocomposite based non-enzymatic hydrogen peroxide sensor. *RSC Advances*, **11**, 19316, 2021. https://doi.org/10.1039/D1RA01485D

[37] Ray, C.; Dutta, S.; Roy, A.; Sahoo, R.; Pal, T. Redox mediated synthesis of hierarchical Bi_2O_3/MnO_2 nanoflowers: A non-enzymatic hydrogen peroxide electrochemical sensor. *Dalton Transactions*, 2016. https://doi.org/10.1039/C6DT00062B